JACS JOURNAL OF THE AMERICAN CHEMICAL SOCIETY

Article

pubs.acs.org/JACS

Electrodeposition of Crystalline GaAs on Liquid Gallium Electrodes in Aqueous Electrolytes

Eli Fahrenkrug,[†] Junsi Gu,[†] and Stephen Maldonado*[,†,‡]

[†]Department of Chemistry and [‡]Program in Applied Physics, University of Michigan, 930 North University, Ann Arbor, Michigan 48109-1055, United States

Supporting Information

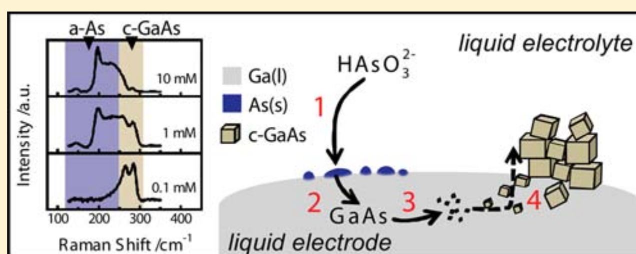

ABSTRACT: Crystalline GaAs (c-GaAs) has been prepared directly through electroreduction of As_2O_3 dissolved in an alkaline aqueous solution at a liquid gallium (Ga(l)) electrode at modest temperatures ($T \geq 80$ °C). Ga(l) pool electrodes yielded consistent electrochemical behavior, affording repetitive measurements that illustrated the interdependences of applied potential, concentration of dissolved As_2O_3, and electrodeposition temperature on the quality of the resultant c-GaAs(s). Raman spectra indicated the composition of the resultant film was strongly dependent on both the electrodeposition temperature and dissolved concentration of As_2O_3 but not to the applied bias. For electrodepositions performed either at room temperature or with high (≥0.01 M) concentrations of dissolved As_2O_3, Raman spectra of the electrodeposited films were consistent with amorphous As(s). X-ray diffractograms of As(s) films collected after thermal annealing indicated metallurgical alloying occurred only at temperatures in excess of 200 °C. Optical images and Raman spectra separately showed the composition of the as-electrodeposited film in dilute (≤0.001 M) solutions of dissolved As_2O_3(aq) was pure c-GaAs(s) at much lower temperatures than 200 °C. Diffractograms and transmission electron microscopy performed on as-prepared films confirmed the identity of c-GaAs(s). The collective results thus provide the first clear demonstration of an electrochemical liquid−liquid−solid (ec-LLS) process involving a liquid metal that serves simultaneously as an electrode, a solvent/medium for crystal growth, and a coreactant for the synthesis of a polycrystalline semiconductor. The presented data serve as impetus for the further development of the ec-LLS process as a controllable, simple, and direct route for technologically important optoelectronic materials such as c-GaAs(s).

■ INTRODUCTION

Crystalline gallium arsenide (c-GaAs) possesses many desirable optoelectronic properties suited for solar energy conversion,[1] light and radiation detection,[2] chemical sensing,[3] lighting,[4] and high speed electronics.[5] One considerable challenge with GaAs technologies at scale is the existing methods for the preparation of c-GaAs(s) are energy-, time-, and resource-intensive.[6] For example, molecular beam epitaxy (MBE) and metal−organic chemical vapor deposition (MOCVD) require ultrahigh vacuum (UHV) equipment, highly refined reagents such as arsine gas, and process temperatures in excess of 600 °C.[7,8] Similarly, liquid phase epitaxy (LPE) and the liquid encapsulated Czochralski (LEC) processes rely on temperatures in excess of 700 °C, require complex furnace designs to minimize loss of As(g) at elevated temperatures, and unavoidably result in crystals with high defect densities.[9−12] Accordingly, although single and multijunction GaAs photovoltaics (PV) are the most efficient solar-to-electricity conversion devices to date,[13] GaAs-based PVs require energy payback times on the order of five years.[14] In this regard, simple, low temperature, and nonresource-intensive c-GaAs(s) preparation strategies are appealing.

Previous work in our group has shown that crystalline inorganic semiconductors can be prepared under benchtop conditions by an electrodeposition process in aqueous solutions without any physical or chemical templates. Specifically, liquid metals can be used simultaneously both as a conventional electrodes for electrodeposition and as solvents for crystalline semiconductor growth at room temperature.[15] The advantage of this electrochemical liquid−liquid−solid (ec-LLS) process is the possibility to prepare directly a functional, crystalline semiconductor material without the need for heavily refined precursors, elaborate equipment, and high temperatures. A recent report details how the ec-LLS process can even be leveraged to make active device components, for example, Li^+ battery anodes.[16]

The hypothesis tested in this work is that c-GaAs(s) can be prepared simply via an embodiment of the ec-LLS process with a liquid gallium (Ga(l)) pool that serves simultaneously as an electrode, a solvent, and as a coreactant. In contrast to conflicting previous reports on the electrodeposition of GaAs,[17,18] we posit that c-GaAs(s) can be synthesized

Received: September 24, 2012
Published: December 24, 2012

 © 2012 American Chemical Society

predictably through the electrodeposition of As from dissolved As_2O_3 specifically on a Ga(l) electrode at modest temperatures in water. A series of material characterizations are shown that highlight the critical parameters associated with c-GaAs(s) formation, with an emphasis on Raman analyses to interrogate crystal type and crystallinity because it is directly amenable to fast product analysis at an electrode surface. These cumulative data are discussed in the context of controlling the ec-LLS process and reconciling aspects of the earlier literature on GaAs electrodeposition from aqueous solutions.

EXPERIMENTAL SECTION

Chemicals and Materials. Ga(l) (99.999%) and platinum (Pt) wire (99.9%) were obtained from Alfa Aesar. Prior to use and if visibly apparent, thick oxide films were mechanically removed from Ga pool surfaces via abrasion with a glass pipet tip. For reference, thick oxide films occurred most readily as a result of freezing/thawing Ga(l) pools,[19] as was done here to facilitate removal of electrodeposited films. As_2O_3(s) powder (99.95%, Mallinckrodt), anhydrous Na_2SO_4 (99%, EMD), and NaOH (98%, Fisher) were used as received. H_2O that was obtained from a Barnstead Nanopure III purification system (>18 MΩ cm) was used for all solutions. Ar(g) (99.998%) was obtained from Detroit Metro Welding.

Electrodeposition and Electrochemical Measurements. CHI420A and CHI760C (CH Instruments) workstations were used for electrochemical experiments. All electrochemical data collected below 100 °C were acquired under open atmosphere in 100 mL Pyrex cells with a three electrode configuration featuring a 200 μL Ga(l) pool working electrode, a Pt flag (2 cm^2) counter electrode, and a Pt wire quasi-reference electrode. Due to electrocapillary effects, electrical contact to the working electrode was made through a small piece of platinum mesh/coil connected to a copper wire insulated by polytetrafluoroethylene (PTFE) that was pushed down through the center of the top of the Ga(l) pool. Electrodepositions performed at temperatures exceeding 100 °C were carried out in a custom-built electrochemical reactor pressurized with Ar(g) to 27.5 bar to minimize solvent vaporization. The reactor was purged with a steady flow of Ar(g) for 10 min prior to heating with heat tape at a rate of 1 °C min^{-1}. The anodic wave featured at −1.375 V in voltammetry collected at 30 °C was used to correct all quasi-referenced potentials to the Ag/AgCl couple. Accordingly, all potentials are reported with respect E(Ag/AgCl, sat. KCl). All electrochemical data are plotted with positive currents indicating net reduction processes and negative currents corresponding to net oxidation processes.

Fabrication and Assembly of a Pressurized Electrochemical Cell. The custom pressurized electrochemical reaction vessel was composed of a stainless steel jacketed exterior with isolated electrical, gas, and thermocouple feedthroughs. Reactor bodies, caps, and compression rings were machined from 304 grade stainless steel round stock (McMaster−Carr) and assembled in-house. PTFE round stock (McMaster−Carr) was used to fabricate gaskets for the static pressure seal. Electrical connections were made through a hermetically sealed 4-pin feedthrough (Pascal Technologies) that was vacuum welded through the reactor cap. Each isolated stainless steel pin was attached directly to individual electrodes through a section of PTFE heat-shrink tubing (McMaster−Carr). A 24 in. × 0.5 in. section of heat tape (Amptek) was used to supply and control heat input. Internal cell temperature was monitored with a K-type stainless steel thermocouple probe (Omega Engineering).

Materials Characterization. Powder X-ray diffraction (XRD) was performed using a Bruker D8 Advance X-ray diffractometer with a Cu Kα X-ray source (λ = 1.5406 Å). A 2.0 mm slit width was employed with a sampling rate of 20 data points per degree 2θ at 1 s $point^{-1}$. For XRD heating experiments, as-deposited samples were placed on a standard glass slide that sat on top of a copper heating element embedded in a ceramic heating block. The temperature was controlled via PID feedback with a custom temperature controller (Omega Engineering). Temperature-dependent diffractograms were collected after annealing for 15 min at each temperature point.

High-resolution transmission electron microscopy (HRTEM) and selected area electron diffraction (SAED) were conducted with a JEOL 3011 TEM equipped with a LaB_6 electron source operating at 300 kV. Samples were prepared as follows: first by freezing the Ga(l) electrode immediately after electrodeposition; followed by gently mechanically removing the electrodeposited film with a razor blade; washing the collected material in a plastic vial with CH_3OH(l) (190 proof, ACS spectrophotometric grade, Aldrich); centrifugation for 60 s at 9G; decanting all but 1 mL of the ethanol supernatant; resuspending the particulates by sonication for 60 s; and finally drop-casting 3 μL onto a 400 mesh copper TEM grid coated with an ultrathin carbon support (Ted Pella).

Raman spectra were obtained using a Renishaw RM Series Raman microscope equipped with a Nikon LU Plan 20× objective (NA = 0.4) and edge filters to reject the 785 nm excitation line. The excitation source and CCD detector (578 × 400) were positioned in a 180° backscatter geometry. No polarizing collection optics were used for spectral acquisition. A 785 nm diode laser was used as the incident excitation at a total radiant power of 1.12 mW over a 20 μm^2 spot to minimize local heating of the sample. In a typical spectral collection, the collected signal was integrated for 30 s, and spectra were scan-averaged over five repetitions. Reported Raman data are representative of a collection of spectra acquired over at least 10 spots covering the surface of each measured sample. Time-dependent in situ Raman spectra were collected in a custom PTFE cell that can accommodate horizontally positioned electrodes designed to fit within the working distance of the objective. Single 10 s spectral acquisitions were sequentially acquired with a 0.8 s delay between collections.

Raman Spectra Fitting and Analysis. Raman spectra were fit in Origin 8.0 using >500 fit iterations with a 1×10^{-15} tolerance using a maximum of three peaks corresponding to the transverse and longitudinal optical phonon modes (TO and LO, respectively) and the overtone of the LO mode (2LO). As noted in previous reports,[20−23] the empirical line shape of the LO mode observed in nanocrystalline GaAs exhibits an asymmetric character; therefore, this mode was best fit with an asymmetric double sigmoidal function. The line shapes of both the TO and 2LO modes were best fit with a Voigt function. The full width at half-maximum of the TO mode was constrained to 15 cm^{-1} for all fits.

The phonon confinement (PC) model[22] has been previously used to interpret optical phonon frequency shifts and peak broadening with the effective crystallite size of the GaAs. In this work, estimates from the PC model were used to assess the measured spectral features of the LO mode from electrodeposited c-GaAs. In the PC model, the line shape of the LO phonon mode is given by[22]

$$I(\omega) \cong \int_0^1 \frac{|C(0, \mathbf{q})|^2 d^3\mathbf{q}}{(\omega - \omega(\mathbf{q}))^2 + (\Gamma_0/2)^2} \quad (1)$$

where vector $\mathbf{q}$ is in the units of $2\pi/a$, a is the lattice constant of GaAs (5.653 Å),[24] $d^3\mathbf{q}$ is the volume element in spherical coordinates, and Γ_0 = 3 cm^{-1} is the natural line width for the LO phonon of GaAs.[23] For an isotropic microcrystal, the phonon confinement can be described by a Gaussian weighting function that yields Fourier coefficients:[20]

$$|C(0, \mathbf{q})|^2 = e^{-\mathbf{q}^2 L^2/4a^2} \quad (2)$$

where L is the phonon confinement length. The phonon dispersion curve for GaAs is given by eq 3:[23]

$$\omega(\mathbf{q}) = A + B\cos(\pi \mathbf{q}) \quad (3)$$

where A and B (269.5 cm^{-1} and 22.5 cm^{-1}, respectively) are fitting constants specific to GaAs.

RESULTS

Voltammetry of Ga(l) Electrodes in Alkaline Electrolyte with and without Dissolved As_2O_3. Figure 1 illustrates

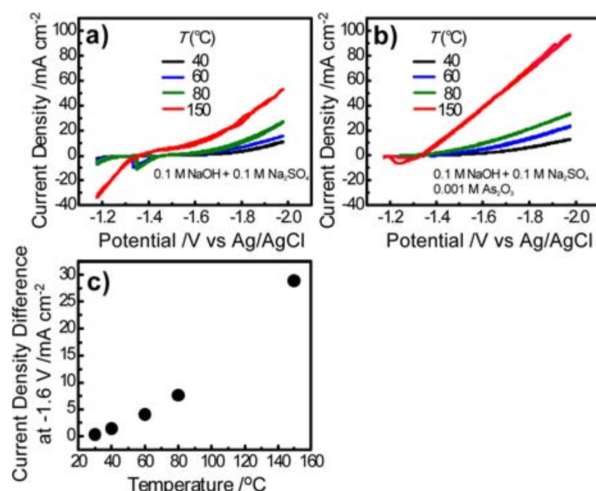

Figure 1. Temperature-dependent cyclic voltammetric responses collected at a Ga(l) pool electrode immersed in an aqueous solution containing (a) 0.1 M NaOH and 0.1 M Na_2SO_4 and (b) 0.1 M NaOH, 0.1 M Na_2SO_4, and 0.001 M As_2O_3. Scan rate: 0.01 V s^{-1}. (c) Difference in measured current density with and without a formal concentration of 0.001 M As_2O_3 in the electrolyte at an applied potential of −1.6 V as a function of temperature.

the current−potential characteristics for Ga electrodes at several temperatures above the melting point (29.8 °C) in an aqueous solution containing 1 mM As_2O_3, 100 mM NaOH, and 100 mM Na_2SO_4. In the absence of dissolved As_2O_3 (Figure 1a), the multielectron oxidation of bulk Ga(l) was observable at potentials more positive than −1.15 V.[25] During scans to potentials more *negative* than the open circuit potential, a separate and "inverted" voltammetric wave (i.e., the current sign implied a net oxidative process during a cathodic sweep) near −1.375 V was noted. Analogous inverted voltammetric waves have been noted previously with metal electrodes that exhibit transpassivity.[25,26] Extended (10 min) potential step experiments with a Ga(l) electrode biased at the peak potential of the inverted voltammetric wave showed a sustained, oxidative process (Supporting Information, Figure S1), arguing against a contaminant dissolved in the electrolyte as the source of this redox process. The linear dependence of the peak current with scan rate (Supporting Information, Figure S2) was consistent with behavior expected from a redox process at the Ga(l) surface. All electrodepositions were performed at potentials more negative than the peak potential for this inverted wave to minimize surface oxides at the Ga(l) interface.

Figure 1b describes the observed voltammetry for a Ga(l) electrode immersed in a solution containing dissolved As_2O_3. At pH = 13, the predominant species in solution was $HAsO_3^{2-}$.[27] At low formal concentrations of As_2O_3, the voltammetric response for sweeps to more negative potentials lacked a well-defined peak. At high (≥50 mM) formal concentrations of As_2O_3, the voltammetric response looked similar but also included a small cathodic wave with a peak at −1.4 V (Supporting Information, Figure S3). The absence of a clear reductive wave indicated an electroreduction at Ga(l) electrodes limited by a kinetic process rather than mass-transport.[28] A similar observation has been made previously for As^{3+} reduction in alkaline solutions at both solid and liquid metal electrodes.[29−31] As a result and as indicated in Figure 1a,b, the difference between current for film formation and H_2(g) evolution was slight at room temperature at low overpotentials. However, at potentials more negative than −1.5 V, the difference between the current measured with and without dissolved As_2O_3 increased. Figure 1c illustrates the competition between the two processes at a given potential was a strong function of temperature, with an apparent increase at higher temperatures of the net difference in measured current density with and without dissolved As_2O_3 in the electrolyte at an applied potential of −1.6 V.

Potential Step Electrodepositions at Room Temperature and High Concentration of Dissolved As_2O_3. Chronoamperometric experiments were performed to effect formation of c-GaAs(s) through As electrodeposition onto Ga(l). To monitor the nature of the deposit, Raman spectra were obtained at the Ga(l)/electrolyte interface during electrodeposition. The first-order Raman spectrum for bulk crystalline GaAs shows two optical phonon modes (TO at 266 cm^{-1} and LO at 292 cm^{-1})[32] that are distinguishable from the primary signatures for amorphous GaAs (150−250 cm^{-1}),[33,34] crystalline As_2O_3 (379, 417, 428, 458, 576, 644, and 750 cm^{-1}),[35,36] amorphous As_2O_3 (450−470 cm^{-1}),[35,36] crystalline As(s) (198 and 257 cm^{-1}),[37−39] and amorphous As(s) (115, 145, 200, 235, 283, and 340 cm^{-1}).[40−42] Figure 2 shows time-dependent Raman spectra for a potential step experiment conducted at room temperature with 40 mM As_2O_3 and an applied bias of −1.0 V. Several signatures were evident after 76 s. Under these electrodeposition conditions, the observed signatures were inconsistent with either crystalline or amorphous GaAs, crystalline or amorphous As_2O_3, and crystalline As(s).[33−42] Instead, the spectral features were uniformly in accord with amorphous As(s).[40−42] The sharpness of the Raman mode at 200 cm^{-1}, as well as the presence of the less intense modes at 115, 145, 283, and 340 cm^{-1}, matched separate reports of amorphous As(s) films with some long-range order (as compared to purely amorphous As(s) films prepared through sputter deposition).[40,41] The intensity of these modes continued to increase monotonically before reaching a maximum after 130 s, consistent with an electrodeposition process that ultimately attains a thickness greater than the Raman probe depth. Similar Raman spectra were collected for As(s) electrodeposition on solid copper electrodes from identical electrolyte solutions (Supporting Information, Figure S4). Raman modes for c-GaAs were never observed during or following potential step experiments to any potential more negative than the open circuit potential with

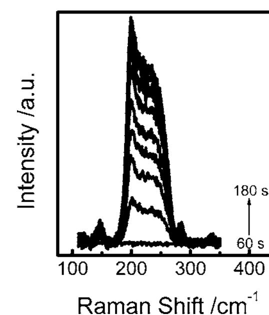

Figure 2. Time-dependent Raman spectra collected every 10.8 s at Ga(l) pool electrodes immersed in an aqueous solution containing 0.1 M NaOH, 0.1 M Na_2SO_4, and 0.04 M As_2O_3 and polarized at −1.0 V. Spectra acquired in first 60 s had no Raman features and are not shown.

Ga(l) electrodes in solutions of 40 mM As_2O_3 at room temperature.

Potential Step Electrodepositions as a Function of Temperature at High Concentrations of Dissolved As_2O_3. Based on the data in Figure 2, additional electrodeposition experiments were performed at higher temperatures to determine whether electroreduction of dissolved As_2O_3 could directly effect c-GaAs(s). Figure 3 contains Raman spectra collected both for electrodeposition experiments held at a constant applied bias and for electrodeposition experiments held at a constant temperature with a Ga(l) electrode immersed in alkaline solution containing a formal concentration of 10 mM As_2O_3. Figure 3a presents Raman spectra collected after electrodeposition at several applied potentials and at a constant temperature of 90 °C. These spectra showed features indicative of only amorphous As(s). At applied potentials more negative than −1.68 V, the evolution of H_2(g) was substantial, mechanically perturbing the as-electrodeposited film. Raman signatures for amorphous As(s) were also observed at this temperature with the Ga(l) electrode at the open-circuit potential (OCP) although the observable film quantity was minimal even after long times ($t \geq 120$ min). The inset in Figure 3b shows an optical image of the amorphous As(s) film on a Ga(l) electrode just after electrodeposition. This characteristic dull black was consistent throughout an electrodeposition (i.e., thin or thick film), transitioning only from pale to progressively more opaque. Figure 3b shows Raman spectra collected for electrodeposited films prepared at various temperatures at a constant bias of −1.58 V. Over the entire temperature range 40−150 °C, the Raman spectra indicated only amorphous As(s) after electrodeposition for two hours. These collective experiments indicated the primary product of electroreduction of dissolved As_2O_3 at high concentrations (10 mM) and elevated temperatures at Ga(l) electrodes was amorphous As(s).

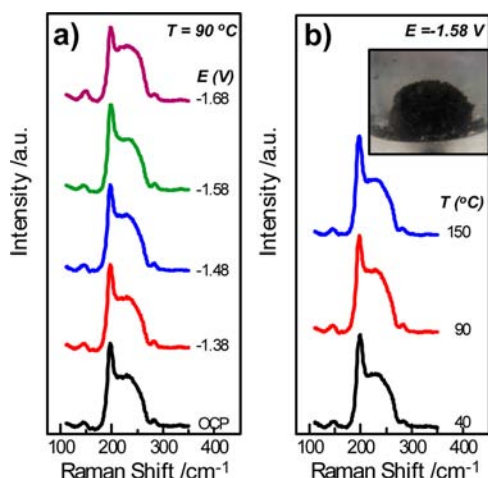

Figure 3. (a) Raman spectra for films deposited at Ga(l) pool electrodes immersed in an aqueous solution containing 0.1 M NaOH, 0.1 M Na_2SO_4, and 0.01 M As_2O_3 at 90 °C for two hours at several different applied biases. For this set of experiments, the OCP was −1.20 V. (b) Raman spectra for films deposited at Ga(l) pool electrodes immersed in an aqueous solution containing 0.1 M NaOH, 0.1 M Na_2SO_4, and 0.01 M As_2O_3 at an applied bias of −1.58 V for two hours at several different electrodeposition temperatures. Spectra are offset for clarity. Inset: Optical photograph highlighting appearance of electrodeposited film at 90 °C at an applied potential of −1.58 V for two hours.

Potential Step Electrodepositions as a Function of Temperature at Low Concentrations of Dissolved As_2O_3. To effectively limit the overall rate and amount of As electrodeposited onto the surface of Ga(l), separate electrodeposition experiments were performed with more dilute concentrations of dissolved As_2O_3. Figure 4 illustrates a time-lapse sequence of optical images of a Ga(l) pool electrode housed in a glass bowl throughout a two hour electrodeposition with an alkaline solution containing a formal concentration of only 1 mM As_2O_3 at 90 °C at an applied bias of −1.58 V. Unlike the dark film featured in the inset of Figure 3, the hue of the electrodeposited film on Ga(l) in this experiment was a uniform gold after 10 minutes. At longer times, the color of the film transitioned through shades of amber, blue, green, and then back to a darker amber. The apparent color of an ultrathin (<100 nm) GaAs film (i.e., the spectral profile of the reflected visible light) should change as the film thickness increases (Supporting Information, Figure S5). The color change stopped if the electrodeposition was stopped, further indicating the color change was a function of the quantity (thickness) of the electrodeposited film. Further experiments confirmed the nature of the electrodeposited film was not amorphous As(s) at lowered concentrations of dissolved As_2O_3. Figure 5 contains Raman spectra for a set of three films electrodeposited at 80 °C at E = −1.58 V onto Ga(l) electrodes immersed in solutions with dissolved As_2O_3 concentrations spanning two orders of magnitude (10−0.1 mM). In Figure 5, the Raman spectra show a transition in the composition of the electrodeposited film from pure amorphous As(s) to pure c-GaAs(s) as the dissolved As_2O_3 concentration decreased. Specifically, the disappearance of the modes associated with amorphous As(s) and the prominent appearance of the TO and LO modes characteristic for c-GaAs(s) were apparent and consistent across the entire film surfaces prepared at 1 and 0.1 mM. The uniformity of the

Figure 4. Optical images of a Ga(l) pool electrode immersed in an aqueous solution containing 0.1 M NaOH, 0.1 M Na_2SO_4, and 0.001 M As_2O_3 at 90 °C while biased at −1.58 V for 0, 30, 60, 90, and 120 min.

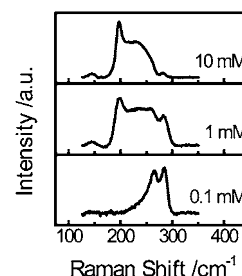

Figure 5. Raman spectra for films deposited at Ga(l) pool electrodes immersed in an aqueous solution containing 0.1 M NaOH, 0.1 M Na_2SO_4 at 80 °C with an applied bias of −1.58 V as a function of the formal concentration of As_2O_3.

spectral features across randomly selected regions on the as-prepared films indicated a homogeneous film composition.

Separate measurements were performed to determine whether the observations in Figures 4 and 5 just reflected a thermal annealing of a thick As(s) layer on Ga(l) at this temperature. Figure 6 summarizes a set of X-ray diffractograms collected after holding a single electrodeposited amorphous As(s) film and Ga(l) pool at several temperatures for 15 min. Reflections at 43.5° and 50.4° in the diffractograms corresponded to the copper heating element positioned beneath the films, and reflections at 25.6° and 29.5° were from the ceramic heating block. XRD data collected for samples with annealing up to 150 °C showed no evidence of crystalline character for GaAs(s). Reflections consistent with zincblende c-GaAs(s) at 27.43°, 45.47°, and 53.87° were only detected in diffractograms collected at 200 °C and above. Analogous annealing experiments analyzed with Raman yielded a similarly high critical annealing temperature (Supporting Information, Figure S6). The measured high threshold temperature necessary for metallurgical alloying of As(s) and Ga(l) into c-GaAs(s) is in accord with previous reports on purposely annealing As and Ga films[18,43−46] and suggest that the data in Figures 4 and 5 obtained far below 200 °C cannot be explained by a simple annealing effect.

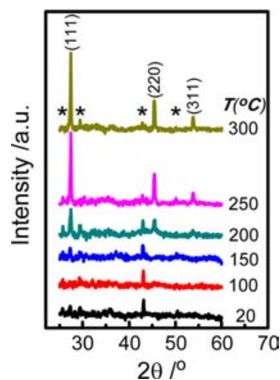

Figure 6. Powder X-ray diffractograms obtained during annealing of an electrodeposited As(s) film on a Ga(l) pool electrode prepared from an aqueous solution containing 0.1 M NaOH, 0.1 M Na_2SO_4, and 0.01 M As_2O_3 at 40 °C. Indexed peaks correspond to zincblende GaAs. Peaks denoted with an asterisk (*) correspond to the copper heating element or the ceramic heating block. Diffractograms are offset for clarity.

Figure 7 displays the temperature- and potential-dependent Raman spectra collected after electroreduction for 120 min in an alkaline solution with a formal As_2O_3 concentration of 1 mM. Raman spectra collected after electrodeposition at a constant temperature of 90 °C showed no clear signatures for amorphous As(s) at any investigated applied potential. Instead, the Raman spectra were dominated by the two peaks for the c-GaAs(s) TO and LO modes centered at 266 and 286.5 cm^{-1}, respectively. At this temperature, changes in the applied potential between −1.48 and −1.68 V did not result in substantial changes in the collected Raman spectra. The number of peaks, peak centers, and peak widths remained unchanged (Table 1). At −1.38 V, the same qualitative spectral features consistent with c-GaAs(s) were apparent, albeit with much lower signal-to-noise. However, the specific applied potential used for electrodeposition did negatively impact the adherence of the c-GaAs(s) film to the Ga(l) electrode surface and reduced the total quantity produced. Experiments performed under the same conditions but in the absence of an applied bias resulted in Raman spectra with no discernible spectral features above the baseline indicating no detectable deposit of any kind.

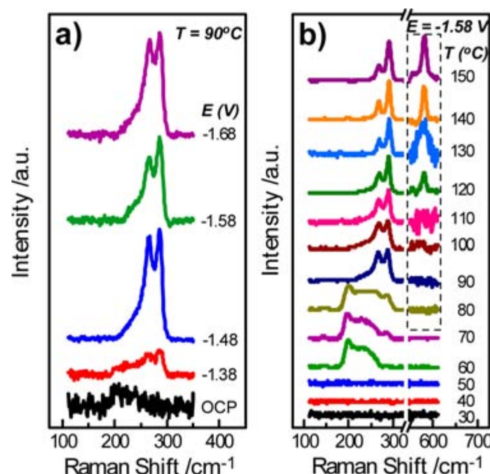

Figure 7. (a) Raman spectra for films deposited at Ga(l) pool electrodes immersed in an aqueous solution containing 0.1 M NaOH, 0.1 M Na_2SO_4, and 0.001 M As_2O_3 at 90 °C for two hours at several different applied biases. For this set of experiments, the OCP was −1.28 V. (b) Raman spectra for films deposited at Ga(l) pool electrodes immersed in an aqueous solution containing 0.1 M NaOH, 0.1 M Na_2SO_4, and 0.001 M As_2O_3 at an applied bias of −1.58 V for two hours at several different electrodeposition temperatures. The dashed box denotes data scaled by an additional factor of 10. Spectra are offset for clarity.

Table 1. Measured Raman Spectral Features for c-GaAs Prepared at Several Applied Potentials[a]

		TO[cd]	LO	TO/LO
conc/ mM	applied potential[b]/V	peak position/ cm^{-1}	peak position/ cm^{-1}	peak intensity ratio
0.1	−1.48	266.1	285.5 (14.1)	100:110
	−1.58	265.8	285.6 (14.8)	100:97
	−1.68	266.1	286.0 (14.4)	100:101
1	−1.38	265.4	285.9 (14.6)	100:117
	−1.48	266.0	286.1 (14.4)	100:106
	−1.58	265.8	285.8 (14.4)	100:134
	−1.68	266.2	286.1 (14.8)	100:107

[a]Prepared at an electrodeposition temperature of 90 °C. [b]Versus Ag/AgCl. [c]Value in parentheses corresponds to fwhm for given peak. [d]Value of fwhm for TO mode constrained to 15 cm^{-1} during peak fitting.

Figure 7b shows representative Raman spectra for electrodeposited films on a Ga(l) electrode prepared in alkaline solution containing 1 mM dissolved As_2O_3 at −1.58 V for 120 min at several temperatures. At or below 50 °C, no Raman features were observed above the background in the collected Raman spectra. At 60 °C, the collected Raman spectra showed the characteristic features for amorphous As(s) only. At 70 °C, the Raman spectra showed more spectral signatures, with a slight peak at 282.5 cm^{-1} consistent with the LO mode for c-GaAs(s) in addition to the modes indicative of amorphous As(s). A similar combination of signatures for both As(s) and c-GaAs(s) was evident in data collected at 80 °C, with an increased intensity and blueshift for the observed c-GaAs(s) LO

dx.doi.org/10.1021/ja309476x | J. Am. Chem. Soc. 2013, 135, 330−339

mode. At 90 °C and higher temperatures, the collected Raman spectra showed only the two prominent c-GaAs(s) TO and LO modes and a total absence of any amorphous As(s) or amorphous GaAs signatures.[33,34,40−42] As the electrodeposition temperature was increased, the collected Raman spectra showed an increase in the relative intensity of the LO mode, a blueshift in the peak center of the LO mode, and a decrease in the full width at half-maximum (fwhm) of the LO mode. These changes are explicitly listed in Table 2. As the electrodeposition temperature increased, the absolute and relative intensities of the first overtone of the LO mode (2LO) at 580 cm^{-1} increased substantially, typically a hallmark of increased crystallite size in a polycrystalline semiconductor sample (vide infra).[47,48]

Table 2. Measured Raman Spectral Features for c-GaAs Prepared at Several Temperatures[a]

		TO^{bc}	LO	2LO	TO/LO/2LO
conc/mM	temp/°C	peak position/cm^{-1}	peak position/cm^{-1}	peak position/cm^{-1}	peak intensity ratio
0.1	80	264.9	284.7 (15.0)	—	100:101:0
	90	265.6	285.6 (14.3)	—	100:111:0
	100	265.3	286.5 (13.3)	—	100:98:0
	110	266.3	287.6 (11.8)	—	100:110:0
	120	266.9	288.5 (11.2)	580.2 (25)	100:112:13
	130	266.7	289.3 (10.7)	579.6 (22)	100:189:12
	140	266.9	289.3 (10.6)	580.0 (18)	100:193:21
	150	267.0	289.3 (10.5)	581.4 (15)	100:215:24
1	80	260.3	284.3 (15.6)	—	100:94:0
	90	265.5	285.4 (14.5)	—	100:106:0
	100	265.9	286.2 (13.6)	—	100:104:0
	110	266.4	287.3 (11.5)	—	100:134:0
	120	266.7	288.1 (10.6)	578.0 (20)	100:182:12
	130	267.2	288.8 (10.7)	579.7 (22)	100:204:13
	140	266.1	288.4 (10.7)	579.4 (15)	100:206:15
	150	267.0	288.5 (10.9)	580.0 (15)	100:246:29

[a]Prepared at an applied potential of −1.58 V vs Ag/AgCl. [b]Value in parentheses corresponds to fwhm for given peak. [c]Value of fwhm for TO mode constrained to 15 cm^{-1} during peak fitting.

Figure 8 shows Raman spectra for c-GaAs(s) films prepared from electrolytes containing 0.1 mM dissolved As_2O_3. As shown in Figure 8a, a negative applied potential of at least −1.48 V was required for deposition of c-GaAs. As observed for films prepared with 1 mM dissolved As_2O_3, changes in the applied potential beyond the threshold for electrodeposition did not impact the measured Raman spectra. All of these spectra showed the same LO and TO features and no signatures for amorphous As(s), irrespective of the applied bias. The Raman spectra in Figure 8b further showed that amorphous As(s) was not deposited at any temperature with 0.1 mM dissolved As_2O_3. At this dissolved As_2O_3 concentration, electrodepositions performed at or below 60 °C did not yield detectable As(s) or c-GaAs(s), and the surface of the Ga(l) electrode showed no visible change. However, at 80 °C and higher, a colored film was deposited onto the Ga(l) electrode. Further, the collected Raman spectra showed that the relative intensities of both the LO and 2LO phonon modes increased at elevated temperatures. The TO peak centers and fwhm values did not vary with electrodeposition temperature.

Crystalline Character of As-prepared c-GaAs Films. Two additional orthogonal analyses were conducted to verify separately the crystallinity of the as-prepared GaAs films. XRD patterns were collected for films electrodeposited at 150 °C (Supporting Information, Figure S7). Reflections indexed to the zincblende unit cell for GaAs were observed in the as-prepared films. Separate electron microscopy data also indicated crystalline character in the electrodeposited films. Figure 9 shows a high-resolution transmission electron micrograph for GaAs prepared at 120 °C in an alkaline solution containing 1 mM As_2O_3. The HRTEM image in Figure

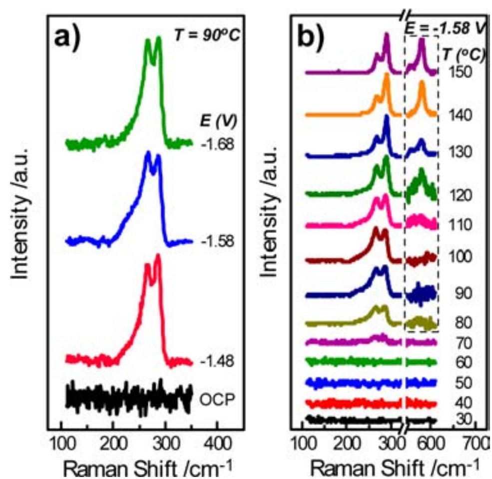

Figure 8. (a) Raman spectra for films deposited at Ga(l) pool electrodes immersed in an aqueous solution containing 0.1 M NaOH, 0.1 M Na_2SO_4, and 0.0001 M As_2O_3 at 90 °C for two hours at several different applied biases. For this set of experiments, the OCP was −1.35 V. (b) Raman spectra for films deposited at Ga(l) pool electrodes immersed in an aqueous solution containing 0.1 M NaOH, 0.1 M Na_2SO_4, and 0.0001 M As_2O_3 at an applied bias of −1.58 V for two hours at several different electrodeposition temperatures. The dashed box denotes data scaled by an additional factor of 10. Spectra are offset for clarity.

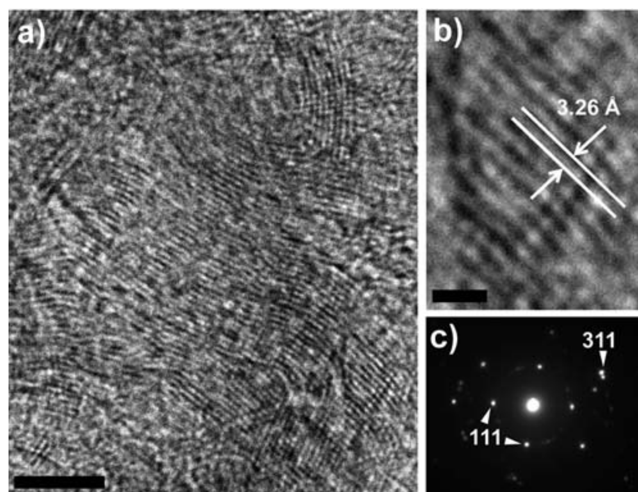

Figure 9. (a) High-resolution transmission electron micrograph of c-GaAs prepared at a Ga(l) pool electrode immersed in an aqueous solution containing 0.1 M NaOH, 0.1 M Na_2SO_4, and 0.001 M As_2O_3 and biased at −1.58 V for 120 min. Scale bar is 5 nm. (b) High-magnification electron micrograph showing lattice fringes with a 3.26 Å spacing. Scale bar is 1 nm. (c) SAED pattern for the same sample in (a). Points positioned on inner and outer rings match expected spacings for zincblende GaAs(111) and (311) planes, respectively.

dx.doi.org/10.1021/ja309476x | J. Am. Chem. Soc. 2013, 135, 330−339

9a displays the lattice fringes with grain sizes around 5 nm. Figure 9b presents a magnified image of a single as-deposited c-GaAs crystallite. The *d*-spacing measured at 3.26 Å from Figure 9b was in accord with the (111) spacing for bulk c-GaAs(s).[24] Figure 9c presents a SAED pattern for the sample shown in Figure 9a,b. The SAED pattern contained diffraction spots that also indexed to the (111) and (311) planes of zincblende GaAs, with measured *d*-spacing values of 3.27 and 1.70 Å, respectively. Corresponding scanning electron micrographs of cross-sectioned samples indicated the GaAs films were approximately 65 nm in thickness (Figure S8, Supporting Information). This thickness value was separately corroborated by inductively coupled plasma (ICP)−atomic emission spectroscopy analysis (Figure S9, Supporting Information).

Figure 10 collects and compares the LO phonon mode features for both sets of spectra in Figures 8b and 7b. Figure 10a summarizes the shift in LO peak position, $\Delta\nu_{LO}$, relative to the LO position for bulk c-GaAs. The two data sets for electrodepositions performed at 1 and 0.1 mM dissolved As_2O_3, respectively, showed comparable values of $\Delta\nu_{LO}$ as a function of temperature up until 120 °C. For electrodeposition temperatures spanning 120−150 °C, the $\Delta\nu_{LO}$ values remained constant for both data sets. Figure 10b shows the relation between $\Delta\nu_{LO}$ and the LO peak fwhm ($fwhm_{LO}$) for the spectra in Figures 8b and 7b. For nanostructured c-GaAs, $\Delta\nu_{LO}$ and $fwhm_{LO}$ are correlated.[23] Figure 10b illustrates the predicted LO phonon shift and fwhm relationship given by the phonon confinement model[49] for a GaAs crystallite with isotropic and Gaussian-type phonon confinement as a function of the phonon confinement length. Following these model parameters, the measured $\Delta\nu_{LO}$ and $fwhm_{LO}$ values for c-GaAs films deposited both in 1 and 0.1 mM dissolved As_2O_3 solutions implied confinement lengths <10 nm in the as-prepared c-GaAs films.

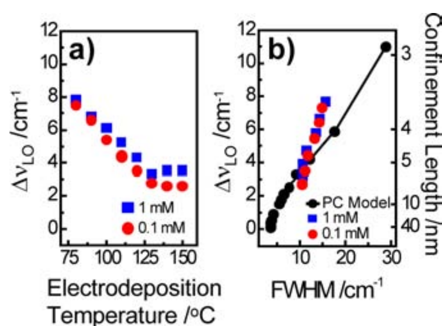

Figure 10. (a) Measured shifts in c-GaAs LO phonon mode ($\Delta\nu_{LO}$) relative to the bulk GaAs LO phonon mode (ν_{LO} = 292 cm^{-1}) as a function of electrodeposition temperature. Electrodeposition conditions were the same as in Figures 6 and 9, with formal concentrations of As_2O_3 of (blue squares) 0.001 M and (red circles) 0.0001 M. (b) Measured c-GaAs LO phonon mode shifts plotted against the measured c-GaAs LO phonon line width. The black line represents the c-GaAs LO phonon shift and peak width relation predicted by the phonon confinement model assuming an isotropic crystal with a Gaussian weighting function. The corresponding confinement length is indicated on the right-hand *y* axis.

■ DISCUSSION

The collected data validate the hypothesis that c-GaAs(s) can be controllably prepared through electroreduction of dissolved As_2O_3 at Ga(l) electrodes at mild temperatures in water. The presented results illustrate that crystallinity in as-prepared GaAs can be achieved without separate thermal annealing. This work represents the first data set describing an ec-LLS process where a liquid metal electrode explicitly serves simultaneously as an electrode, a solvent, and a coreactant to produce a crystalline binary semiconductor. The key aspects impacting this ec-LLS process for GaAs are a clean Ga(l)/electrolyte interface, a sufficiently negative bias to reduce dissolved As_2O_3, a low concentration of dissolved As_2O_3, and temperatures much lower than typically seen in established wet chemical inorganic syntheses.[50−52] These points are detailed below.

Observed Factors Affecting the GaAs ec-LLS Process. The measurements shown here indicate controllable and predictable behavior of Ga(l) electrodes in this GaAs ec-LLS process. For example, a set of 10 replicate electrodepositions at 80 °C and an applied bias of −1.58 V in 1 mM As_2O_3 solutions produced films identical in color, crystallinity, and quantity (i.e., nominal measured film mass = 0.025 mg). Although Ga(l) electrodes have been previously noted as less reproducible than Hg(l) electrodes for electroanalytical applications,[25,53] the consistency of the voltammetric responses collected here support the contention that Ga(l) electrodes are not compromised by thick, blocking films in this electrolyte at the employed potentials. Specifically, we posit that the passivating oxides (≤10 Å) previously noted on Ga(l) surfaces exposed to air through X-ray reflective measurements were not stable at the negative applied biases used here.[54,55] Three empirical observations are in accord with a pristine Ga(l)/electrolyte interface for the conditions employed here. First, the linear scan rate dependence of the inverted voltammetric wave suggests a surface-based process. Second, the sustained anodic current implies continuous Ga(l) dissolution at the peak potential of the inverted voltammetric wave. Third, the potential of the inverted voltammetric wave is proximal to the transition potential from corrosion susceptibility to stability for Ga(l) electrodes predicted by electrode potential−pH equilibrium diagrams.[55,56] We posit that potential-dependent removal of a passivating oxide film exposes the surface of bare Ga(l) to electrolyte and is thus unstable until sufficiently negative applied potentials. Additionally, the appearance and shape of the Ga(l) pool electrodes were inconsistent with an interface dictated by surface oxides. Ga(l) pools exposed to humid air attain a slightly dull, gray appearance and appear semiflat (compressed). Upon immersion in these alkaline electrolytes, Ga(l) pool surfaces attained a crisp, mirror finish with a convex contour, in accord with literature descriptions of the increased a surface tension/shape of a Ga(l) pool following removal of an interfacial oxide(s).[57,58]

The synthesis of c-GaAs(s) shown here required an applied bias substantially more negative than −0.982 V, which is the standard potential of the $HAsO_3^{2-}$/As redox couple. In all experiments where the electrochemical cell was charged with both Ga(l) and dissolved As_2O_3 but no bias was applied, c-GaAs(s) was not observed. At all concentrations and at temperatures below 50 °C, there was no visible or detectable film deposited on the Ga(l) pool. At high dissolved As_2O_3 concentrations and high temperatures, a film composed exclusively of amorphous As(s) was detectable by Raman spectroscopy. Accordingly, the available evidence clearly indicates that electroreduction of As_2O_3 to As(s) is a key and necessary step in this preparation of c-GaAs(s). However, the impact that the *rate* at which As(s) is electrodeposited onto Ga(l) is less clear.

In a cathodic electrodeposition process under kinetic control, the two principle factors that govern the rate (J_{dep}, expressed as a current density) of material deposition are the concentration of the reducible species (C) and the applied bias (E_{app}) used to perform the electroreduction:

$$J_{dep} = nFCk^0 e^{-\alpha F(E^0 - E_{app})/RT} \tag{4}$$

where J_{dep} is the measured electrodeposition current density, k^0 is the standard rate constant for electroreduction of the species being deposited, α is the charge-transfer coefficient, E^0 is the standard potential for the species to be deposited, and the other terms have their usual electrochemical meanings.[28] Equation 4 follows a Butler–Volmer formalism and should be generally valid for the data shown here, since none of the voltammetry for the electroreduction of dissolved As_2O_3 indicated a transition to mass-transport limited conditions (i.e., a "peak" in the net voltammetric response for As_2O_3 electroreduction). Equation 4 predicts that the electrodeposition rate is a stronger function of the applied bias than the dissolved As_2O_3 concentration. However, the collected data implicate the dissolved As_2O_3 concentration as the factor that more strongly determined whether c-GaAs(s) was formed over amorphous As(s). Specifically, at a given temperature, a transition in the composition of the resultant film on the Ga(l) electrode from amorphous As(s) to c-GaAs(s) occurred as the formal concentration of As_2O_3 was varied by two orders of magnitude. However, at a given temperature and formal As_2O_3 concentration, variation in the applied bias by as much as 0.3 V did not change any measurable feature in the Raman spectra, that is, the apparent film composition was the same. Assuming a nominal transfer coefficient of 0.5, a 0.3 V change in the applied potential should also effect approximately a two orders of magnitude increase in the rate of electrodeposition. The apparent rate of film electrodeposition as inferred from visible inspection did increase at more negative potentials. Accordingly, the data suggest the absolute rate of As(s) electrodeposition was not itself a primary controlling factor in facilitating this ec-LLS process.

Description of the GaAs ec-LLS Process. One alternative possibility regarding the apparently strong sensitivity of the formation of c-GaAs toward the concentration of dissolved As_2O_3 is that the concentration of dissolved As_2O_3 could more directly impact the *form* of the initial electrodeposit. The dissolving power of a liquid melt toward a solid is sensitive to the morphology of the solid.[59] At a constant mass, a solid will dissolve more quickly and readily when presented as a fine, high surface area powder rather than a single, large object. Specifically, for any binary system composed of a solid dissolving into a liquid, the rate of dissolution of the solid into the liquid phase is given by eq 5:[60]

$$\frac{dC}{dt} = k_{diss}\frac{s}{V}(C_{sat} - C_{diss}) \tag{5}$$

where k_{diss} is the dissolution rate constant, s is the surface area of the solid in contact with the liquid, V is the volume of the liquid, C_{sat} is the solubility of the solid in the liquid, and C_{diss} is the concentration of the dissolved solid in the bulk of the liquid phase. In the case of electrodeposition, the morphology of deposited films begins typically as discrete nuclei/islands.[61] After sufficient time, the discrete clusters coalesce and eventually form a continuous phase. At a given applied potential, the size, density, and average spacing of the initial electrodeposited clusters can depend on several factors. Analytical expressions are known for interpreting these parameters from chronoamperometric data for electrodepositions performed under mass-transport limitations.[62−64] Although equivalent expressions have not been determined for electrodepositions performed under purely kinetic limitations,[61] similar functional forms are expected with parameters such as concentration. Notably, the island density of electrodeposited films scales as $C^{3/2}$.[61] Accordingly, electrodepositions performed at higher concentrations will generally be both faster and have high nucleation densities that can coalesce into a continuous film quickly. A coalesced film should result in low effective s/V for the electrodeposited solid. Conversely, electrodeposition in more dilute solutions will not only deposit more slowly but also result in less dense, discretized amorphous islands that favor larger s/V ratios.

We hypothesize that subsequent formation of c-GaAs(s) requires controlled dissolution of As(s). At room temperature, the equilibrium solubility of As in Ga is sparing (10^{-13} atom %).[65,66] The binary phase diagram for Ga and As mixtures indicates that the equilibrium mixture composition at high mole fractions of Ga is Ga(l) and GaAs(s).[67] As a result, formation first of a stable, solvated As species within Ga(l) is not expected. Instead, the formation of dissolved GaAs most likely occurs as a result of, or concomitant with, As(s) dissolution. Precipitation of c-GaAs(s) should then follow earlier ec-LLS descriptions,[15,16] where crystallization results from supersaturation of the liquid metal electrode with GaAs. Assuming classical nucleation theory,[68] the size of the precipitating nuclei from a supersaturated solution should increase at higher temperatures where solubility is greater. The increase in effective domain size implied by the blueshifts and narrowed peak widths in collected Raman spectra at higher temperatures supports this general premise.

Figure 11 summarizes the proposed ec-LLS model for GaAs. The multistep sequence inherently places a large emphasis on

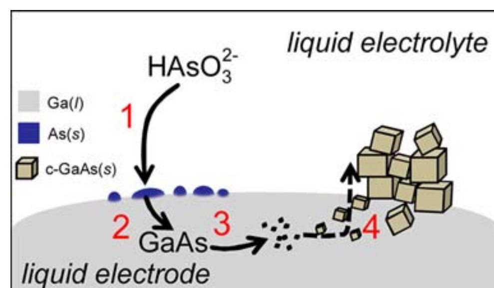

Figure 11. Schematic depiction of the GaAs ec-LLS process constituted by four principal steps. (1) Electroreduction of dissolved As_2O_3 to As(s) at the Ga(l) pool electrode surface. (2) Dissolution of As(s) into the Ga(l) pool and concurrent alloying to form an intermetallic GaAs phase. (3) Crystallite nucleation of dissolved GaAs. (4) c-GaAs crystal growth and phase separation from Ga(l).

the interplay between the individual electrochemical, chemical, metallurgical, and physical growth steps. If As(s) is electrodeposited in a manner that exceeds the dissolution and alloying reaction rates, then an excess of amorphous As(s) will accumulate and prevent formation of c-GaAs as the primary product at any temperature. If As(s) is electrodeposited in a fashion that facilitates fast dissolution into Ga(l) and reaction to form GaAs, then c-GaAs(s) will ultimately be produced.

dx.doi.org/10.1021/ja309476x | J. Am. Chem. Soc. 2013, 135, 330−339

According to the collected data, the crystalline grain size, as inferred from the Raman measurements, of the resultant c-GaAs(s) follows temperature more strongly than changes in dissolved As_2O_3 concentration and applied potential.

GaAs ec-LLS Process Outlook and Context. This work demonstrates the proof of concept of the GaAs ec-LLS process but does not define the full extent of which this tactic can be leveraged. A more quantitative development of the interplay between the various processes identified in Figure 11 is needed. Accordingly, a better understanding of several aspects of the operation of liquid metal electrodes is paramount. First, electrodeposition at liquid metal electrodes is not comprehensively understood. On solid electrodes, the role of adatom surface diffusion on the electrodeposited nuclei density, size, and shape has only recently been recognized.[69,70] Electrodeposition studies with liquid metal electrodes, where surface transport could be fast, have yet to address this aspect.[71,72] Second, chemical dissolution and reaction rate constants at the interface between solid and liquid metals are not well described. Although discussed in the context of solders,[59] a more comprehensive understanding of these rate constants would give greater predictive power in designing better ec-LLS processes. Third, nucleation within and crystal growth out of a liquid metal electrode under applied bias is not well described. Liquid phase epitaxial crystal growth at high temperatures (>850 °C) and under large current densities (2−10 A cm^{-2}) has been attempted,[73] but the analogies between that process and this ec-LLS sequence have yet to be established. Further, as implied by eq 5, the physical properties of the liquid metal should impact the ec-LLS process. More work is needed to identify how features relating to the physical size/shape of the liquid metal electrode influence the c-GaAs produced through the ec-LLS process. In this preliminary stage, we have observed that c-GaAs shows some innate n-type responsivity to white light illumination (Supporting Information, Figure S10). However, it is unclear whether this observation is an intrinsic property of this particular GaAs ec-LLS process or is a result of extrinsic measurements conditions. A better understanding of the microscopic role of Ga(l) in this ec-LLS process is necessary. In addition, identification of other low melting point metals and metal alloys that could be employed as liquid metal electrodes for ec-LLS would be useful to synthesize other crystalline binary and/or ternary semiconductors.

The work presented here not only represents an explicit demonstration of an ec-LLS process for GaAs but also provides insight to rationalize the existing GaAs electrodeposition literature. Most reports indicate that coelectrodeposition of Ga and As from aqueous electrolytes cannot yield c-GaAs without subsequent annealing at high temperatures ($T \geq 250$ °C).[18,43−46] Typically, the net product at room temperature of coelectrodeposition of Ga and As is an amorphous, physical mixture of Ga and As. However, select reports do indicate some level of crystallinity in GaAs(s) from Ga and As coelectrodeposition at mild temperatures.[17,74,75] In coelectrodeposition, it is possible that microscopic Ga(l) droplets are formed initially that could then facilitate some type of ec-LLS process as described here. We have recently demonstrated that the ec-LLS process is in fact possible with discrete metal nanoparticles.[16] As the data here show, the ec-LLS strategy for GaAs is sensitive to many processes, and unless each is tightly regulated, a high yield of highly crystalline GaAs at mild temperatures is difficult. Still, the development of electrochemical reactors that exploit this particular ec-LLS process represents an exciting new strategy for preparing GaAs-based technologies.

CONCLUSIONS

The cumulative data show that c-GaAs(s) can be directly electrodeposited on Ga(l) pool electrodes in aqueous solutions under mild conditions without requiring annealing, expensive precursors, or multiple process steps. Raman spectroscopy, powder XRD and TEM analyses independently and collectively confirmed the c-GaAs films are polycrystalline as prepared. The salient feature of this work is the demonstration of an ec-LLS sequence where a liquid metal serves simultaneously as an electrode substrate, a crystal growth solvent/medium, *and* a coreactant for the electrochemical preparation of c-GaAs from dissolved oxides in water. The data shown here establish a precedent for an alternative methodology for the preparation of c-GaAs that does not require vacuum or high-temperature equipment, potent gaseous precursors, or exotic solvents. Based on these, the future work to develop this process to produce functional c-GaAs materials and devices is outlined.

ASSOCIATED CONTENT

Supporting Information

Additional experimenal details; chronoamperometric and scan rate dependent voltammetry data for the observed "inverted" voltammetric wave; current−potential characteristics for a Ga(l) electrode in 50 mM As_2O_3; Raman spectral data for As(s) electrodeposited at Cu(s); Raman spectra collected during in situ heating experiments; ICP analysis of As quantity; model results of the reflectance−wavelength profiles expected for thin GaAs films; a powder X-ray diffractogram for an as-prepared GaAs film; scanning electron micrographs; and a representative photoelectrochemical response of electrodeposited c-GaAs films under white light illumination. This material is available free of charge via the Internet at http://pubs.acs.org.

AUTHOR INFORMATION

Corresponding Author

smald@umich.edu

Notes

The authors declare no competing financial interest.

ACKNOWLEDGMENTS

Acknowledgment is made to the donors of the American Chemical Society Petroleum Research Fund (51339-DNI5) for support of this research. E.F. acknowledges a University of Michigan Rackham Merit Fellowship. J.G. recognizes the University of Michigan Chemistry Department for Research Excellence Award fellowship. The authors separately thank J. Leddy and S. Boettcher for informative and stimulating discussions and R. Wentz for assistance with cell design. The JEOL 3011 TEM instrument used in this work was maintained by the University of Michigan Electron Microbeam Analysis Laboratory through NSF support (DMR-0315633).

REFERENCES

(1) Bosi, M.; Pelosi, C. *Prog. Photovoltaics* **2007**, *15*, 51.

(2) Buttar, C. M. *Nucl. Instrum. Methods Phys. Res., Sect. A* **1997**, *395*, 1.

(3) Charlton, C.; Giovannini, M.; Faist, J.; Mizaikoff, B. *Anal. Chem.* **2006**, *78*, 4224.

(4) Hayashi, I.; Panish, M. B.; Foy, P. W.; Sumski, S. *Appl. Phys. Lett.* **1970**, *17*, 109.

(5) Hung, H. L. A.; Hegazi, G. M.; Lee, T. T.; Phelleps, F. R.; Singer, J. L.; Huang, H. C. *IEEE Trans. Microwave Theory Tech.* **1988**, *36*, 1966.
(6) Cowley, A. H.; Jones, R. A. *Angew. Chem., Int. Ed. Engl.* **1989**, *28*, 1208.
(7) Nakanisi, T. *J. Cryst. Growth* **1984**, *68*, 282.
(8) Manasevi, H. *Appl. Phys. Lett.* **1968**, *12*, 156.
(9) Jurisch, M.; Eichler, S. In *3rd Czochralski Symposium*, Kcynia, Poland, 2003.
(10) Thomas, R. N.; Hobgood, H. M.; Eldridge, G. W.; Barrett, D. L.; Braggins, T. T.; Ta, L. B.; Wang, S. K. *Semicond. Semimetals* **1984**, *20*, 1.
(11) Weiner, M. E.; Lassota, D. T.; Schwartz, B. *J. Electrochem. Soc.* **1971**, *118*, 301.
(12) Hicks, H. G. B.; Manley, D. F. *Solid State Commun.* **1969**, *7*, 1463.
(13) Green, M. A.; Emery, K.; Hishikawa, Y.; Warta, W.; Dunlop, E. D. *Prog. Photovoltaics* **2012**, *20*, 12.
(14) Mohr, N. J.; Schermer, J. J.; Huijbregts, M. A. J.; Meijer, A.; Reijnders, L. *Prog. Photovoltaics* **2007**, *15*, 163.
(15) Carim, A. I.; Collins, S. M.; Foley, J. M.; Maldonado, S. *J. Am. Chem. Soc.* **2011**, *133*, 13292.
(16) Gu, J.; Collins, S. M.; Carim, A. I.; Hao, X.; Bartlett, B. M.; Maldonado, S. *Nano Lett.* **2012**, *12*, 4617.
(17) Chandra, S.; Khare, N. *Semicond. Sci. Technol.* **1987**, *2*, 214.
(18) Yang, M. C.; Landau, U.; Angus, J. C. *J. Electrochem. Soc.* **1992**, *139*, 3480.
(19) Chabala, J. M. *Phys. Rev. B* **1992**, *46*, 11346.
(20) Campbell, I. H.; Fauchet, P. M. *Solid State Commun.* **1986**, *58*, 739.
(21) Huang, Y. H.; Yu, P. Y.; Charasse, M. N.; Lo, Y. H.; Wang, S. *Appl. Phys. Lett.* **1987**, *51*, 192.
(22) Richter, H.; Wang, Z. P.; Ley, L. *Solid State Commun.* **1981**, *39*, 625.
(23) Tiong, K. K.; Amirtharaj, P. M.; Pollak, F. H.; Aspnes, D. E. *Appl. Phys. Lett.* **1984**, *44*, 122.
(24) Cho, A. Y.; Dernier, P. D. *J. Appl. Phys.* **1978**, *49*, 3328.
(25) Varadharaj, A.; Rao, G. P. *Proc. - Indian Acad. Sci., Chem. Sci.* **1990**, *102*, 177.
(26) Stirrup, B. N.; Hampson, N. A. *J. Electroanal. Chem.* **1976**, *67*, 45.
(27) Tomilov, A. P.; Smetanin, A. V.; Chernykh, I. N.; Smirnov, M. K. *Russ. J. Electrochem.* **2001**, *37*, 997.
(28) Bard, A. J.; Faulkner, L. R. *Electrochemical Methods*, 2nd ed.; John Wiley & Sons: Chichester, U.K., 2004.
(29) Arnold, J. P.; Johnson, R. M. *Talanta* **1969**, *16*, 1191.
(30) Bayerle, V. *Recl. Trav. Chim. Pays-Bas* **1925**, *44*, 514.
(31) Bejan, D.; Bunce, N. J. *J. Appl. Electrochem.* **2003**, *33*, 483.
(32) Abstreiter, G.; Bauser, E.; Fischer, A.; Ploog, K. *Appl. Phys.* **1978**, *16*, 345.
(33) da Silva, S. W.; Lubyshev, D. I.; Basmaji, P.; Pusep, Y. A.; Pizani, P. S.; Galzerani, J. C.; Katiyar, R. S.; Morell, G. *J. Appl. Phys.* **1997**, *82*, 6247.
(34) Desnica, I. D.; Ivanda, M.; Kranjcec, M.; Murri, R.; Pinto, N. *J. Non-Cryst. Solids* **1994**, *170*, 263.
(35) Ashby, C. I. H.; Sullivan, J. P.; Newcomer, P. P.; Missert, N. A.; Hou, H. Q.; Hammons, B. E.; Hafich, M. J.; Baca, A. G. *Appl. Phys. Lett.* **1997**, *70*, 2443.
(36) Li, X.; Bohn, P. W. *J. Electrochem. Soc.* **2000**, *147*, 1740.
(37) Calleja, J. M.; Lannin, J. S.; Cardona, M.; Schonher., E. *Bull. Am. Phys. Soc.* **1974**, *19*, 227.
(38) Schwartz, G. P.; Dutt, B. V.; Gualtieri, G. J. *Appl. Phys. Lett.* **1981**, *39*, 52.
(39) Schwartz, G. P.; Schwartz, B.; Distefano, D.; Gualtieri, G. J.; Griffiths, J. E. *Appl. Phys. Lett.* **1979**, *34*, 205.
(40) Lannin, J. S. *Bull. Am. Phys. Soc.* **1976**, *21*, 461.
(41) Lannin, J. S. *Phys. Rev. B* **1977**, *15*, 3863.
(42) Nemanich, R. J.; Lucovsky, G.; Pollard, W.; Joannopoulos, J. D. *Solid State Commun.* **1978**, *26*, 137.
(43) Gheorghies, C.; Gheorghies, L.; Fetecau, G. *J. Optoelectron. Adv. Mater.* **2007**, *9*, 2795.
(44) Mahalingam, T.; Lee, S.; Lim, H.; Moon, H.; Kim, Y. D. *Sol. Energy Mater.* **2006**, *90*, 2456.
(45) Kozlov, V. M.; Bozzini, B.; Bicelli, L. P. *J. Alloys Compd.* **2004**, *379*, 209.
(46) Mengoli, G.; Musiani, M. M.; Paolucci, F. *J. Electroanal. Chem.* **1992**, *332*, 199.
(47) Wagner, J.; Hoffman, C. *Appl. Phys. Lett.* **1987**, *50*, 682.
(48) Hardtdegen, H.; Hollfelder, M.; Meyer, R.; Carius, R.; Munder, H.; Frohnhoff, S.; Szynka, D.; Luth, H. *J. Cryst. Growth* **1992**, *124*, 420.
(49) Gouadec, G.; Colomban, P. *Prog. Cryst. Growth. Ch.* **2007**, *53*, 1.
(50) Beberwyck, B. J.; Alivisatos, A. P. *J. Am. Chem. Soc.* **2012**, in press.
(51) Harrison, B. C.; Tompkins, E. H. *Inorg. Chem.* **1962**, *1*, 951.
(52) Wells, R.; Pitt, C.; McPhail, A.; Purdy, A.; Shafieezad, S.; Hallock, R. *Chem. Mater.* **1989**, *1*, 4.
(53) Lezhava, T. I.; Vagramyan, A. I. *Russ. Chem. Bull.* **1964**, *13*, 409.
(54) Korshunov, V. N.; Safonov, V. A. *Russ. J. Electrochem.* **2001**, *7*, 1089.
(55) Pourbaix, M. *Atlas of Electrochemical Equilibria*, 2nd ed.; National Association of Corrosion Engineers: Houston, TX, 1974.
(56) Pourbaix, M. *Biomaterials* **1984**, *5*, 122.
(57) Dickey, M. D.; Chiechi, R. C.; Larsen, R. J.; Weiss, E. A.; Weitz, D. A.; Whitesides, G. M. *Adv. Funct. Mater.* **2008**, *18*, 1097.
(58) Larsen, R. J.; Dickey, M. D.; Whitesides, G. M.; Weitz, D. A. *J. Rheol.* **2009**, *53*, 1305.
(59) Dybkov, V. I. *Reaction Diffusion and Solid State Chemical Kinetics*; IPMS: Kyiv, Russia, 2002.
(60) Dokoumetzidis, A.; Macheras, P. *Int. J. Pharm.* **2006**, *321*, 1.
(61) Guo, L.; Oskam, G.; Radisic, A.; Hoffmann, P. M.; Searson, P. C. *J. Phys. D: Appl. Phys.* **2011**, *44*, 44301.
(62) Palomar-Pardave, M.; Scharifker, B. R.; Arce, E. M.; Romero-Romo, M. *Electrochim. Acta* **2005**, *50*, 4736.
(63) Scharifker, B.; Hills, G. *Electrochim. Acta* **1983**, *28*, 879.
(64) Scharifker, B.; Mostany, J. *J. Electroanal. Chem.* **1984**, *177*, 13.
(65) Hall, R. N. *J. Electrochem. Soc.* **1963**, *110*, 385.
(66) Thurmond, C. D. *J. Phys. Chem. Solids* **1965**, *26*, 785.
(67) Tmar, M.; Gabriel, A.; Chatillon, C.; Ansara, I. *J. Cryst. Growth* **1984**, *69*, 421.
(68) Kumar, S.; Nann, T. *Small* **2006**, *2*, 316.
(69) Guo, L.; Searson, P. C. *Electrochim. Acta* **2010**, *55*, 4086.
(70) Radisic, A.; Vereecken, P. M.; Hannon, J. B.; Searson, P. C.; Ross, F. M. *Nano Lett.* **2006**, *6*, 238.
(71) Astley, D. J.; Harrison, J. A. *Electrochim. Acta* **1970**, *15*, 2007.
(72) Fleischmann, J.; Harrison, J. A.; Thirsk, H. R. *Trans. Faraday Soc.* **1965**, *61*, 2742.
(73) Bryskiewicz, T.; Boucher, C. F.; Lagowski, J.; Gatos, H. C. *J. Cryst. Growth* **1987**, *82*, 279.
(74) Gao, Y. K.; Han, A. Z.; Lin, Y. Q.; Zhao, Y. C.; Zhang, J. D. *J. Appl. Phys.* **1994**, *75*, 549.
(75) Murali, K. R.; Subramanian, V.; Rangarajan, N.; Lakshmanan, A. S.; Rangarajan, S. K. *J. Mater. Sci.: Mater. Electron.* **1991**, *2*, 149.